ELSEVIER

Ceramics International 27 (2001) 431–441

CERAMICS INTERNATIONAL

www.elsevier.com/locate/ceramint

A manometric method for the determination of chemical diffusion in perovskite-type cathode materials of the solid oxide fuel cell

S.P.S. Badwal [a], S.P. Jiang [a], J. Love [b], J. Nowotny [c,*], M. Rekas [c], E.R. Vance [d]

[a] *CSIRO, Manufacturing Science and Technology, Private bag 33, Clayton South MDC, Clayton, Victoria 3169, Australia*
[b] *Ceramic Fuel Cell Limited, 170 Browns Road, Noble Park, Victoria 3174, Australia*
[c] *Centre for Materials Research in Energy Conversion, School of Materials Science and Engineering, The University of New South Wales, Sydney, NSW 2052, Australia*
[d] *Australian Nuclear Science and Technology Organisation, Lucas Heights, NSW 2234, Australia*

Received 18 May 2000; received in revised form 23 May 2000; accepted 29 August 2000

Abstract

This paper describes a manometric method for the determination of chemical diffusion coefficients from gas/solid equilibration kinetics for electrode materials of the type (La,Sr)(Mn,Fe,Co)O_3. The equilibration kinetics was monitored by measurements of the $p(O_2)$ changes during a reaction between oxygen and the electrode material involving both oxidation and reduction experiments in the temperature range 773–1123 K. Activation energy of the chemical diffusion measurements at different temperatures was determined during both oxidation and reduction experiments. The chemical diffusion coefficients measured by the present manometric method on $La_{0.8}Sr_{0.2}MnO_{3-\delta}$ have been compared with those reported in the literature.

Keywords: C. Diffusion; D. Perovskite; Manometric method; SOFC

1. Introduction

For the development of solid oxide fuel cell technology, intensive research has been carried out on the characterisation of oxide electrode materials, such as (La,Sr) MnO_3 (LSM), (La,Sr)CoO_3 (LSC), (La,Sr)FeO_3 (LSF) and their solid solutions. The studies have focused on the determination of oxygen conduction, defect chemistry and kinetics of oxygen transfer process at the electrode/electrolyte interface [1–17]. With the aim to develop an oxide material with optimized properties required of an electrode material, specifically high oxygen-ion conductivity, low over-potential losses for the oxygen transfer reaction across the electrode/electrolyte interface and low reactivity with solid electrolytes (e.g. doped zirconia), a study has been undertaken to determine the chemical diffusion coefficient of oxygen in LSM, LSC, LSF and their solid solutions [18]. Also surface electrical properties of these materials have been examined in terms of the charge transfer kinetics at the gas/solid interface [19].

The chemical diffusion data reported in literature are essentially limited to the data of Beltzner et al. [1,5]. They have observed a substantial scatter of data (within 2 orders of magnitude) in the temperature range 980–1040 K. Hammouche et al. [2] reported only one value at 1230 K.

This paper describes a manometric method for monitoring the gas/solid equilibration kinetics and its application for the determination of the chemical diffusion coefficient in perovskite-type electrode materials, (LaSr)(Mn,Fe,Co)O_3. This method was then used to determine diffusion data over a wide temperature range of LSM, LSC and LSF. This paper reports diffusion data for $(La_{0.8}Sr_{0.2})MnO_3$.

2. Definition of terms

2.1. Non-stoichiometry

$LaMnO_3$ (also $LaCoO_3$, $LaFeO_3$) is known to exhibit non-stoichiometry with respect to oxygen. This non-

* Corresponding author. Tel.: +61-2-9385-6465; fax: +61-2-9385-6467.
E-mail address: j.nowotny@unsw.edu.au (J. Nowotny).

0272-8842/01/$ - see front matter
PII: S0272-8842(00)00098-5

stoichiometry may be substantially increased by the introduction of acceptors, such as Sr, into the La sublattice.

Mn ions in $LaMnO_3$ are tri-valent (Mn^{3+}). $LaMnO_3$ may be doped with Sr within a wide range of concentrations. Sr-doped $LaMnO_3$, that is p-type semiconductor, exhibits both Mn^{+3} and Mn^{+4} ions. Their ratios depend on $p(O_2)$. The precise information on the relationship between the crystal structure and the defect chemistry is somewhat ambiguous for such materials, however, we have made the plausible assumption that the predominant type of defects in this compound are Sr_{La}' ions, introduced into A-sites and forming acceptor centres, and electron holes, $Mn_{\bullet n}$. Its minor ionic defects are oxygen vacancies, at low $p(O_2)$, or cation vacancies, at high $p(O_2)$. In both cases its minor electronic defects are electrons. Concordantly, the general formula of Sr-doped $LaMnO_3$, in which the ratio of the cations at A-sites to the cations at B-sites equals unity, should be expressed as $(La_{1-x}Sr_x)MnO_{3-\delta}$. In the low $p(O_2)$ regime δ assume a positive value and corresponds to oxygen deficiency in the oxygen sublattice. Then the predominant defects are oxygen vacancies. In the high $p(O_2)$ regime δ assumes negative values which correspond to an apparent oxygen excess. Then the predominant defects are cation vacancies.

The charge neutrality condition for Sr-doped $LaMnO_3$ may be expressed as:

$$[Sr'_{La}] + 3[V'''_{La}] + 3[V'''_{Mn}] + n = 2[V_{\ddot{O}}] + p \quad (1)$$

where n and p denote the concentration of electrons and electron holes, respectively.

Fig. 1 illustrates the effect of Sr on defect concentrations in LSM. Defect chemistry and related electrical properties of LSM have been reported in Ref. [17].

2.2. Equilibration kinetics

Equilibrium in the metal oxide/oxygen system, and related defect concentrations in oxide crystals, are determined by oxygen activity in the gas phase and temperature. When one of these parameters is changed then the system tends to achieve a new equilibrium state. Thus the reequilibration, involving the transition between two equilibrium states, may be performed either isothermally, when a new equilibrium is imposed by suddenly changed $p(O_2)$, or isobarically when a sudden change of temperature is imposed at a constant $p(O_2)$ [20].

When $p(O_2)$ is changed to a new value (within a single phase region) over an initially equilibrated oxide crystal, then a new non-stoichiometry (and related concentration of defects) is imposed at the surface almost immediately. The new non-stoichiometry is then propagated into the crystalline bulk to regain new chemical potentials throughout the crystal. The rate of the propagation is determined by chemical diffusion [20].

In the case of perovskite-type oxide materials, such as $(La_{1-x}Sr_x)MnO_{3-\delta}$, the mobility of oxygen vacancies is larger than that of cation vacancies [19]. However, the

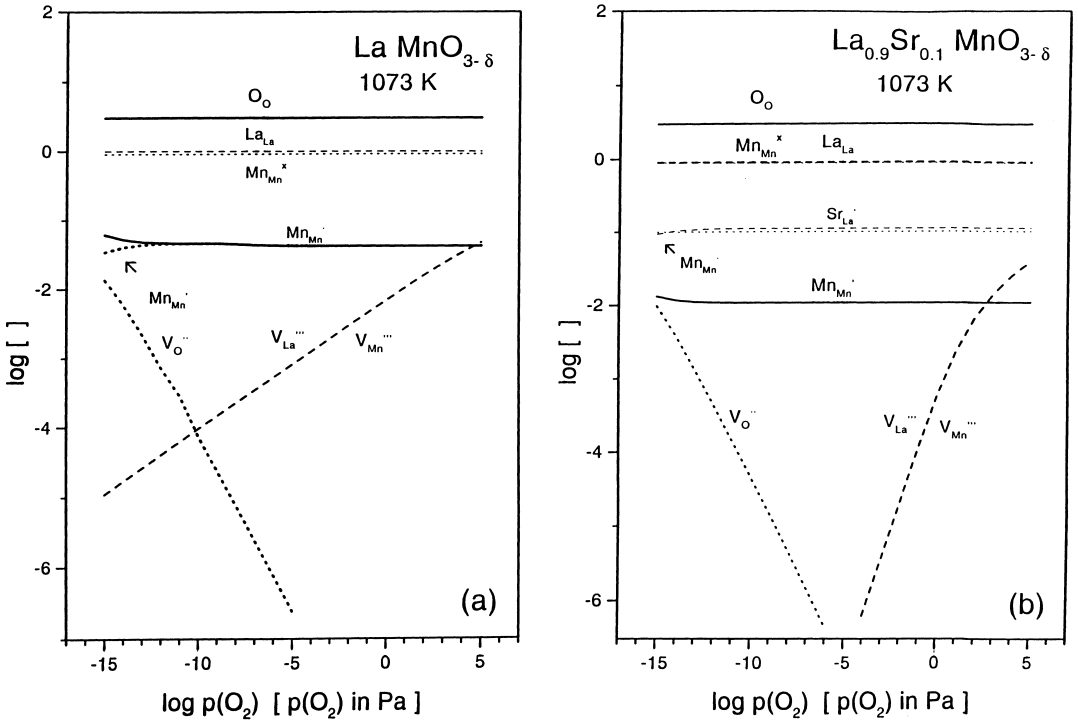

Fig. 1. The concentration of defects as a function of $p(O_2)$ in undoped $LaMnO_3$ (a) and Sr-doped $LaMnO_3$ (b) [17].

diffusion flux of the cation sublattice may assume substantial values during the equilibration in the high $p(O_2)$ regime (Fig. 1b).

The oxidation/reduction equilibration process may be expressed by the following reaction:

$$(La_{1-x}Sr_x)MnO_{3-\delta} + \frac{\Delta\delta}{2}O_2 \rightleftarrows (La_{1-x}Sr_x)MnO_{3-\delta+\Delta\delta} \quad (2)$$

The equilibration process in oxide systems can be monitored by changes of a bulk crystal property, such as weight, electrical conductivity, thermoelectric power, work function, etc., that is sensitive to non-stoichiometry. Alternatively the amount of oxygen that is consumed (or evolved) can be measured by a technique such as the manometric method, used in the present study, to gain information about the oxidation/reduction equilibrium kinetics. The application of the manometric method in monitoring the equilibration kinetics as well as the applied kinetic equations are described below.

2.3. Chemical diffusion coefficient

The chemical diffusion coefficient was determined from approximate solutions of Fick's second law derived by Price and Wagner [20]. For a long equilibration time, corresponding to large values of the equilibration degree, γ, the logarithmic equation is applicable:

$$\log(1-\delta) = \log\left(\frac{8}{\pi^2}\right) - \frac{\pi^2 Dt}{2.303(4r^2)}. \quad (3)$$

where D is the chemical diffusion coefficient, t is time, r is radius of a sphere-shape grain. The equilibration degree is defined as:

$$\gamma = \frac{\Delta p_t}{\Delta p_\infty} \quad (4)$$

Δp_t and Δp_∞ denote changes of $p(O_2)$ after time t and the time after new equilibrium is reached, respectively. For small values of the equilibration degree the parabolic equation is applicable:

$$\gamma^2 = \frac{Dt}{\pi}\left(\frac{2q}{v}\right)^2 \quad (5)$$

where q and v denote surface area and volume of the grain or specimen, whatever is applicable.

2.4. Impact of non-stoichiometry on transport

Eqs. (3) and (5) are valid when $0.75 < \gamma < 0.99$ and $0 < \gamma < 0.5$, respectively. Essentially, both kinetic equations should provide the same values of the diffusion coefficient, if the non-stoichiometry is low, its change during the equilibration process is small and the transport mechanism is independent of the non-stoichiometry. Then, there is an excellent agreement between the diffusion data determined from the logarithmic Eq. (3) and general diffusion equation [21] if one transport mechanism and kinetics is predominant during the entire equilibration process. This indeed is the case for compounds exhibiting a very low non-stoichiometry, such as NiO, in which the concentration of defects remains in the range 0.001–0.01 at.%. However, in the case of the perovskite-type oxide materials, such as LSM, LSC and LSF, the concentration of defects may assume substantial values (Fig. 1). Then interactions between the defects, and their mobility, do change substantially during the equilibration process.

As seen from Fig. 1 the predominant defects in oxidised and reduced LSM are cation vacancies and oxygen vacancies, respectively. As also seen their concentration does change markedly with oxygen activity. Accordingly, one should expect that the chemical diffusion coefficient determined from Eqs. (3) and (5) may assume different values during both reduction and oxidation as it was observed by Kononchuk et al. [22]. In this case Eqs. (3) and (5) provide information about the chemical diffusion coefficient at low and high values of the equilibration degree, respectively.

3. Statement of the problem

Sr-doped lanthanum manganite is most commonly used cathode material in solid oxide fuel cells due to its reasonable electronic conductivity, high stability with respect to the zirconia based electrolytes, and high charge transfer rates for oxygen across the electrode/electrolyte interface. However, LSM exhibits very low oxygen-ion conduction [4,7]. Therefore, high porosity of the electrode materials, based on LSM, is required for optimum three phase boundary area between electrode, electrolyte and the gas phase and thus for efficient transfer of oxygen from the gas phase to the surface of the electrolyte [23].

Substitution of Mn in LSM with Co or with Fe results in a substantial increase of oxygen-ion conduction through the electrode material which, therefore, reduces the requirement for large three phase boundary area. Unfortunately, a substantial disadvantage of both LSC and LSF is their high reactivity with zirconia based electrolyte and their high thermal expansion coefficient relative to other fuel cell components [23].

There have been an accumulation of diffusion data for the air electrode materials reported in literature [1–8]. Their comparison is difficult as often these data have different physical meaning (e.g. the self diffusion coefficient, the diffusion coefficient of oxygen vacancies and the chemical diffusion coefficient). Furthermore, there is less consistency between materials used by different authors with respect to compositions, concentration of impurities and microstructure. Accordingly, the objective of the present study, reported in this work and the following papers [18,19], is to perform a uniform characteristics of electrode materials, with respect to the equilibration kinetics, within a wide range of compositions including LSM, LSC, LSF and their solid solutions.

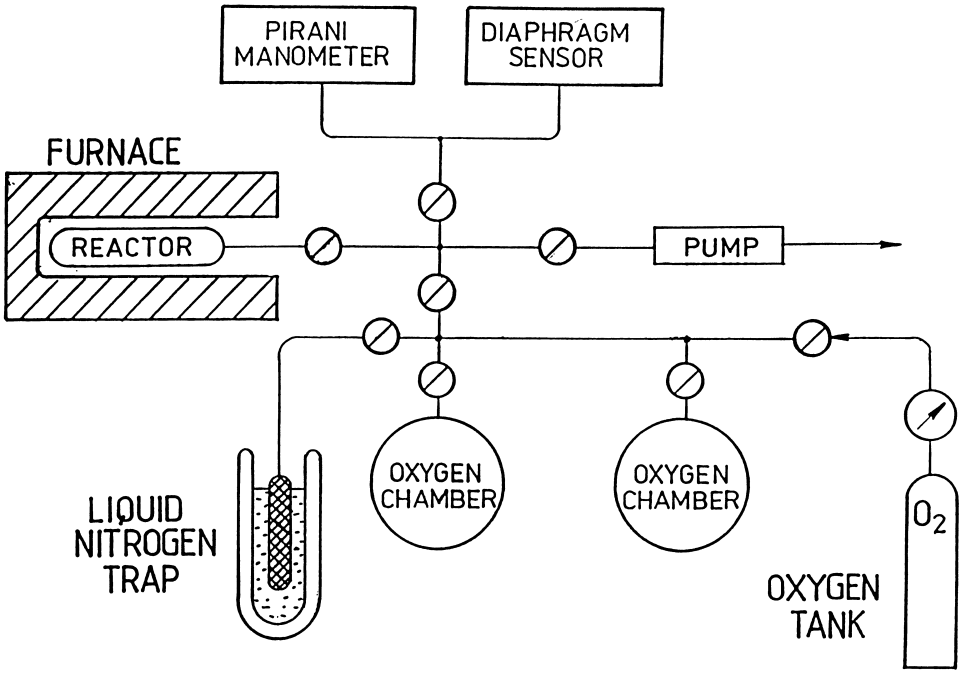

Fig. 2. Schematic illustration of the equipment used for manometric determination of the chemical diffusion coefficient.

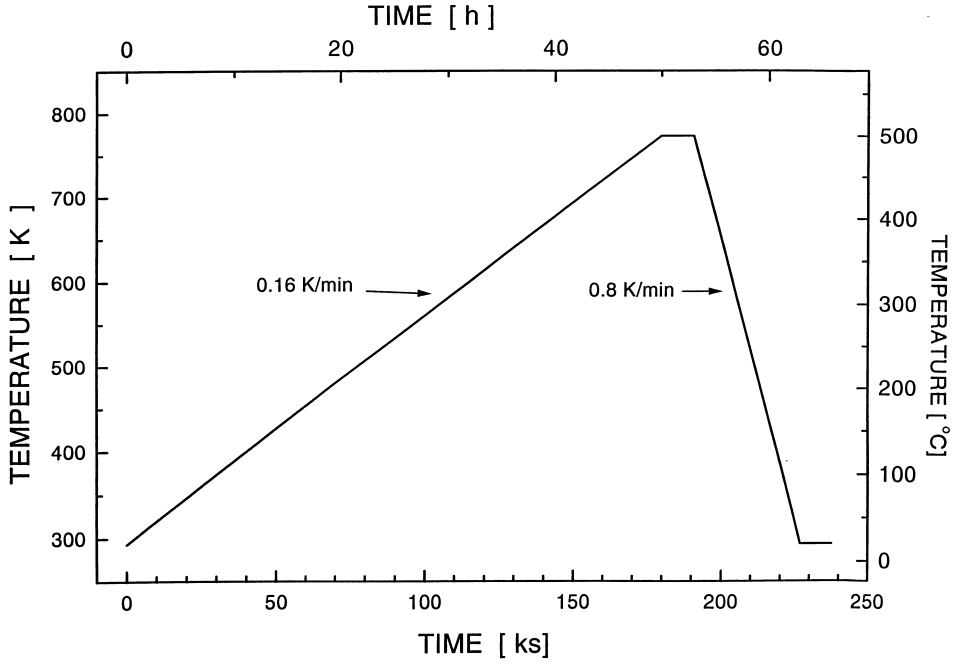

Fig. 3. The temperature program applied in annealing of the LSM specimen.

4. Experimental procedures

4.1. The manometric method

In the manometric method the progress of a chemical reaction, such as oxygen incorporation into an oxide specimen, can be monitored by the determination of changes in $p(O_2)$. The oxidation or reduction of an oxide specimen would result in a decrease or an increase in $p(O_2)$ respectively in the gas phase. Assuming that these changes are negligibly small the equilibration process can be considered as quasi-isobaric.

Fig. 2 illustrates the apparatus, made of glass, which was used in the present study. A manometer, which covers a wide range of pressures, was installed at the reaction chamber. The manometer involved two types of pressure sensors: a diaphragm sensor, operating in the range 200 Pa– 200 kPa, and a Pirani-type sensor, working in the range 0.1–200 Pa. The pressure could be recorded with an accuracy of up to 0.1 Pa. A liquid nitrogen trap served to remove traces of water vapour from the gas phase.

The temperature of the specimen was measured using a thermocouple located at the specimen. However, another thermocouple, steering the temperature control system, was also employed and located near the heating element.

The equilibration experiments were performed isothermally within both oxidation and reduction runs. The oxidation experiments involved successive sudden imposition of an increased $p(O_2)$ over an initially equilibrated specimen. This sudden increase in $p(O_2)$ was followed by a decrease in $p(O_2)$ due to oxygen consumption by the oxide specimen. The rate of this decrease was monitored by the measurement of the $p(O_2)$ changes as a function of time. The reaction volume was adjusted in such a way that overall $p(O_2)$ changes during oxygen consumption remained within 10% of the initial $p(O_2)$ value. Consequently, the experimental conditions can be considered as quasiisobaric.

In analogy to the oxidation experiments, the reduction experiments involved successive sudden imposition of decreased $p(O_2)$. This was achieved by pumping out the reaction chamber. Imposition of reduced $p(O_2)$ was followed by an increase in $p(O_2)$ due to oxygen evolvement from the oxide specimen.

4.2. Specimen preparation

The $(La_{0.8}Sr_{0.2})MnO_3$ (LSM) powder was prepared by co-precipitation process followed by calcination at 1000°C in air for 24 h. XRD examination did not reveal a presence of a second phase in the calcined powder and, consequently, there was no indication of unreacted starting materials. The powder was iso-pressed into discs and sintered at 1250°C in air for 6 h. The dimension of the specimen was generally 8 mm in diameter and 3.83 mm in thickness. In order to remove the moist without destruction the pellets the specimens were slowly heated (0.16 K min^{-1}) up to 773 K and then

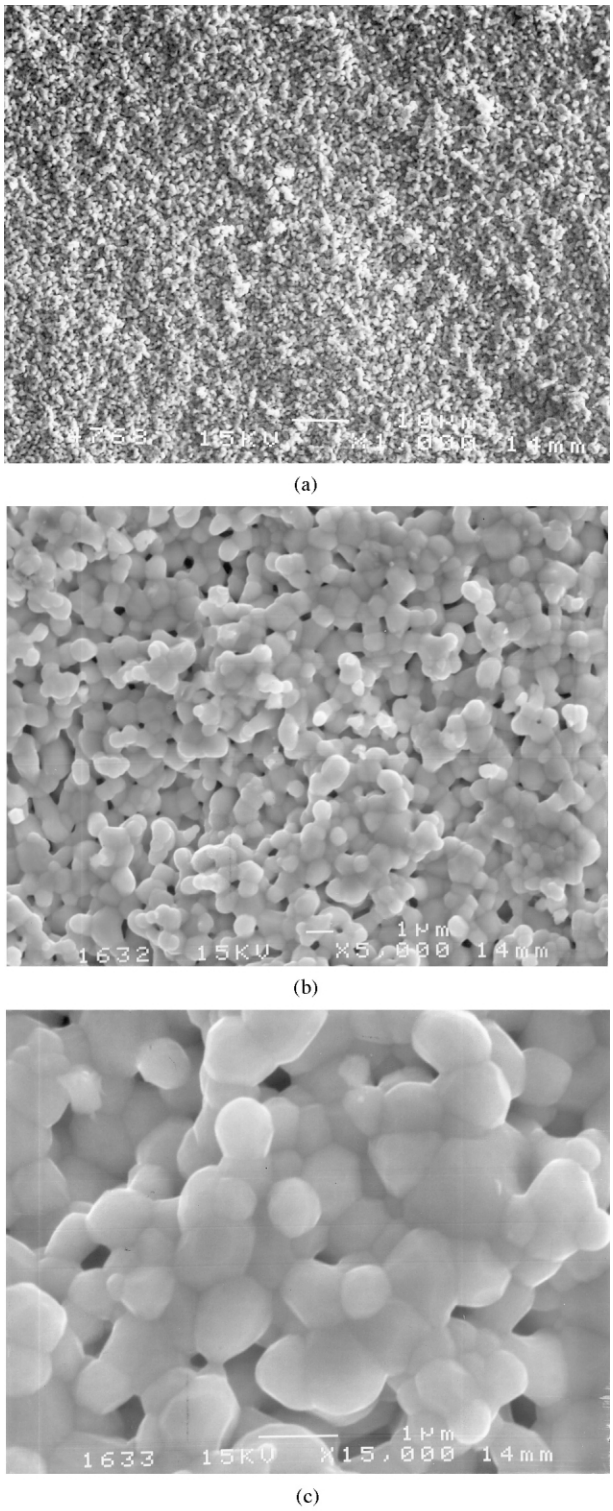

(a)

(b)

(c)

Fig. 4. The SEM micrograph of the LSM specimen; a, b and c correspond to enlargements 1700, 5000 and 15,000, respectively.

slowly cooled (0.8 K min^{-1}) in air. Fig. 3 illustrates the applied temperature program.

The SEM picture of the LSM specimen is shown in Fig. 4. As seen the average grain size is approximately 0.6 μm.

4.3. Procedures

The experimental procedure involved (i) evacuation the reactor (with the specimen) at room temperature down to pressure of about 1 Pa, (ii) heating it under 1 Pa

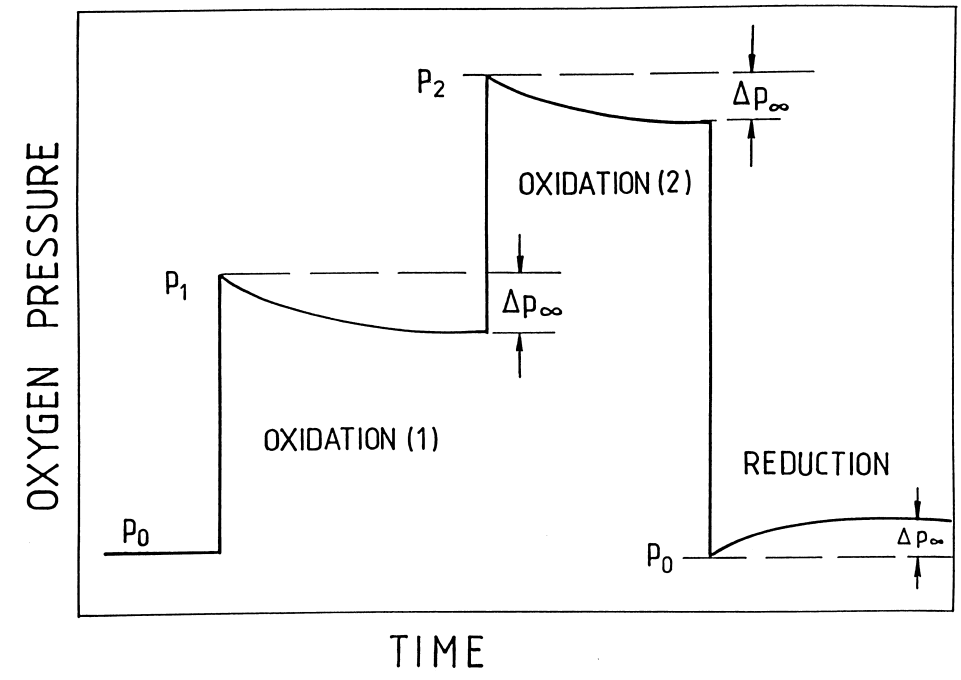

Fig. 5. Schematic illustration of the $p(O_2)$ changes during oxidation and reduction runs, involving imposition of the initial pressure and its subsequent changes as a function of time.

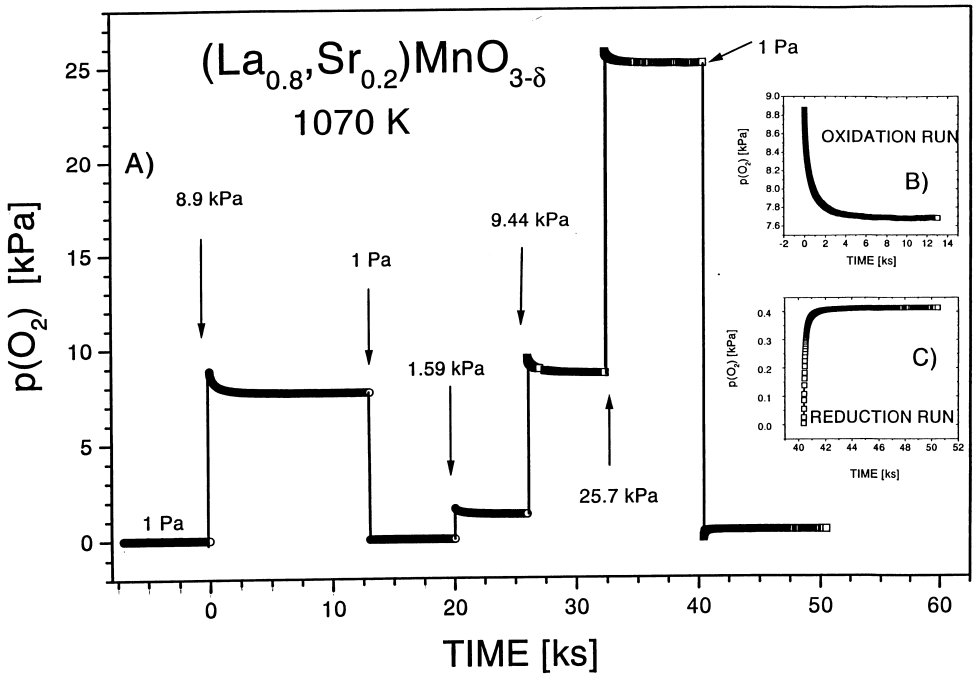

Fig. 6. The changes of $p(O_2)$ within several consecutive oxidation and reduction experiments for $(La_{0.8}Sr_{0.2})MnO_3$ at 1070 K; B and C show enlarged effects within oxidation and reduction runs, respectively.

to 1070 K, and (iii) changing the temperature to the desired level under the same pressure of 1 Pa. Following this procedure, the $p(O_2)$ in the reaction chamber was isothermally increased (oxidation) and from that moment, $p(O_2)$ changes in the specimen chamber were monitored as a function of time. The procedure of imposing of an increased $p(O_2)$ was very fast (1–2 s). The sudden increase of $p(O_2)$ resulted in an increase of oxygen consumption by the specimen which led to a slow decrease in $p(O_2)$ in time by Δp_∞. The oxidation runs were performed within several steps, involving individual experiments, where $p(O_2)$ was increased up to 30 kPa.

In analogy the reduction experiments were performed involving a sudden outgassing of the reaction chamber to a lower $p(O_2)$. This results in evolvement of oxygen from the specimen and, consequently, in a slow increase of $p(O_2)$ in time. The reduction runs, performed successively, resulted ultimately in a decrease of $p(O_2)$ to the level of 1 Pa.

Fig. 5 illustrates schematically the experimental procedure involving the $p(O_2)$ changes during two oxidation runs, when oxygen is step-wise increased from p_o to p_2 and one reduction run when oxygen pressure is lowered from p_2 to p_o. Fig. 6 shows the changes of $p(O_2)$ within several consecutive oxidation and reduction experiments for LSM at 1070 K.

Fig. 7 shows changes of $p(O_2)$ during respective runs of oxidation and reduction for LSM at 1070 K. As seen, in the case of oxidation the pressure changes remain within 5% of the initial $p(O_2)$, however, these were large enough to allow monitoring of the reaction kinetics as a function of time.

5. Results and discussion

5.1. Equilibration kinetic data

The obtained experimental data of the equilibration degree, γ, as a function of time are shown in Fig. 8 for both oxidation and reduction runs. The γ values were calculated according to Eq. (4).

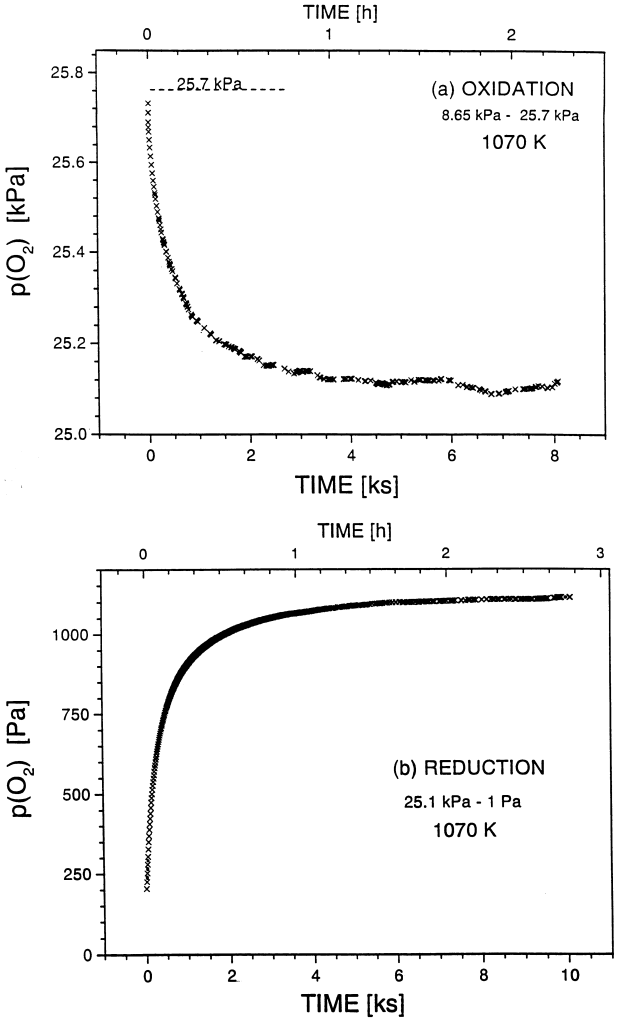

Fig. 7. Changes of $p(O_2)$ as a function of time during oxidation (a) and reduction (b) experiments for $(La_{0.8}Sr_{0.2})MnO_3$ at 1070 K.

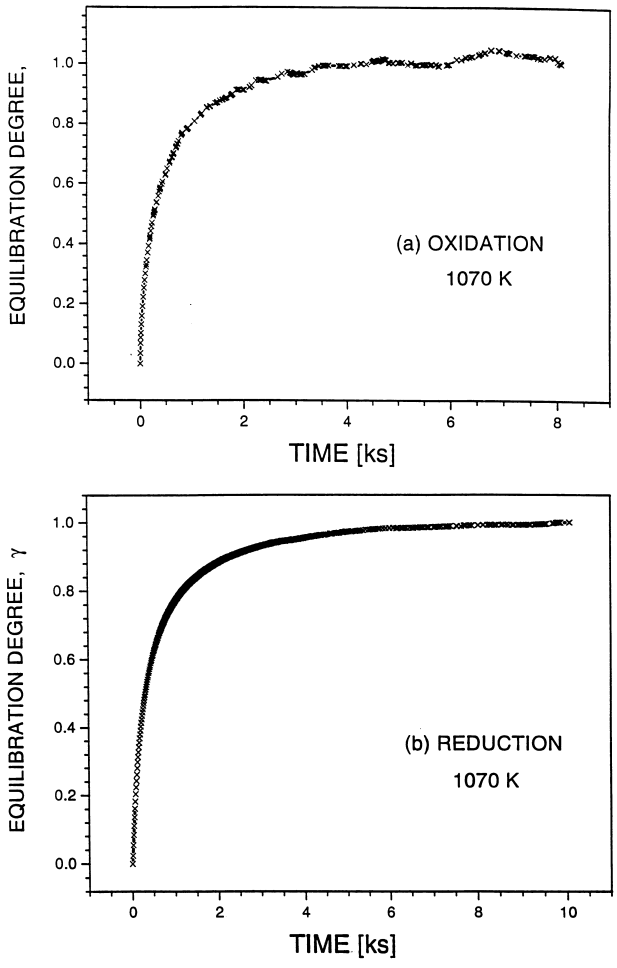

Fig. 8. Changes of the equilibration degree (γ) as a function of time during oxidation (a) and reduction (b) experiments for $(La_{0.8}Sr_{0.2})MnO_3$ at 1070 K.

The plots of γ^2 as a function of time for both oxidation and reduction runs are shown in Fig. 9. As seen the experimental data exhibit a linear dependence in the range $0.05 \leqslant \gamma \leqslant 0.5$. According to parabolic Eq. (5) the slope of the linear part is equal to $(D/\pi)(2q/v)^2$. From the slope, one can obtain the chemical diffusion coefficient, D_{par} where subscript par indicates the parabolic equation used.

Fig. 10 shows the plots of $\log(1-\gamma)$ as a function of time for both oxidation and reduction runs. As seen the experimental data exhibit a linear dependence in the range $0.7 \leqslant \gamma \leqslant 0.99$. According to logarithmic Eq. (3) the slope of the linear part is equal to $-(D\pi^2)/(2.303 \times 4r^2)$. Similar to D_{par}, one can calculate $D_{\log}$.

The diffusion data for LSM were determined, using both kinetic Eqs. (3) and (5), in the temperature range 500–850°C.

5.2. Equilibration mechanism

The chemical diffusion coefficient can be determined from the equilibration kinetic data, if the mechanism of the equilibration process is well known. Specifically, it is important to know whether the equilibration is rate controlled by (i) the transport through individual grains, while the grain boundary transport is very fast, or (ii) the bulk transport through the slab of the specimen. In order to establish this, we determined the equilibration kinetics for two slabs of the same specimen composition but with a different thickness. Fig. 11 shows the difference between the equilibration rate constants B^R and B^S, defined by Eqs. (6) and (7), for over 40 individual experiments of oxidation and reduction:

$$B_{\text{par}} = \frac{D}{\pi}\left(2\frac{q}{v}\right)^2 \tag{6}$$

$$B_{\log} = \frac{\pi^2 D}{4r^2 2.303} \tag{7}$$

where superscripts R and S correspond to the rate constants of a reduced thickness (1.18 mm) and standard thickness (3.83 mm) specimens, respectively, and subscripts par and log correspond to the kinetic Eqs. (5) and (3), respectively. As seen the rate constants B_{par} and $B_{\log}$ are independent of the specimen thickness. This

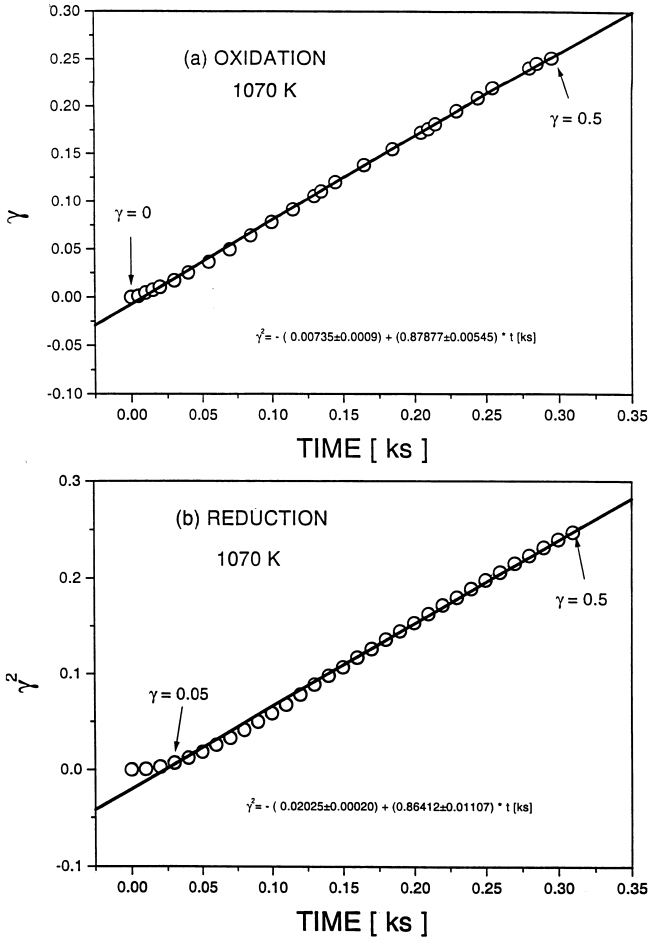

Fig. 9. The plots of γ^2 as a function of time for oxidation (a) and reduction (b) runs at 1070 K.

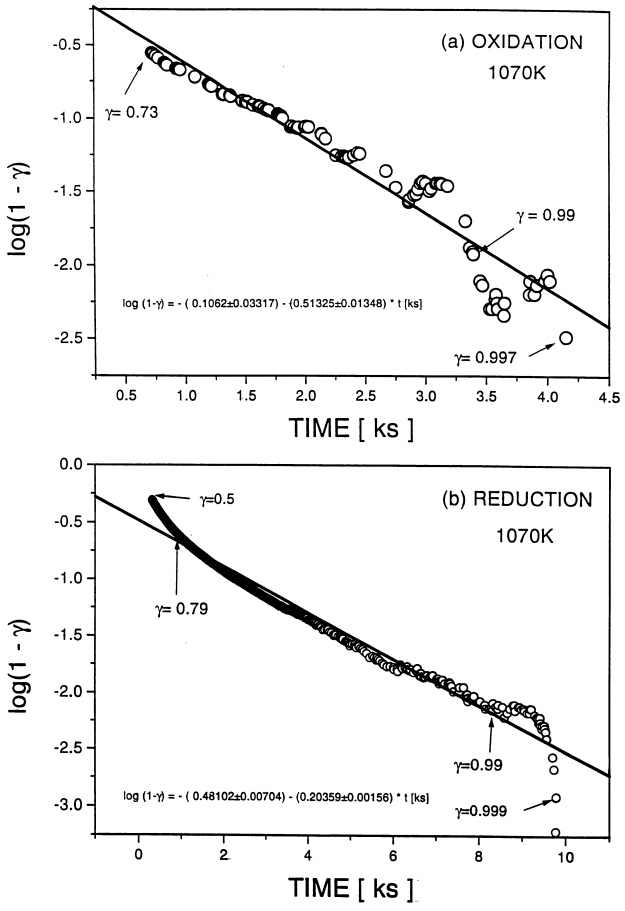

Fig. 10. The plots of $\log(1-\gamma)$ as a function of time for oxidation (a) and reduction (b) runs at 1070 K.

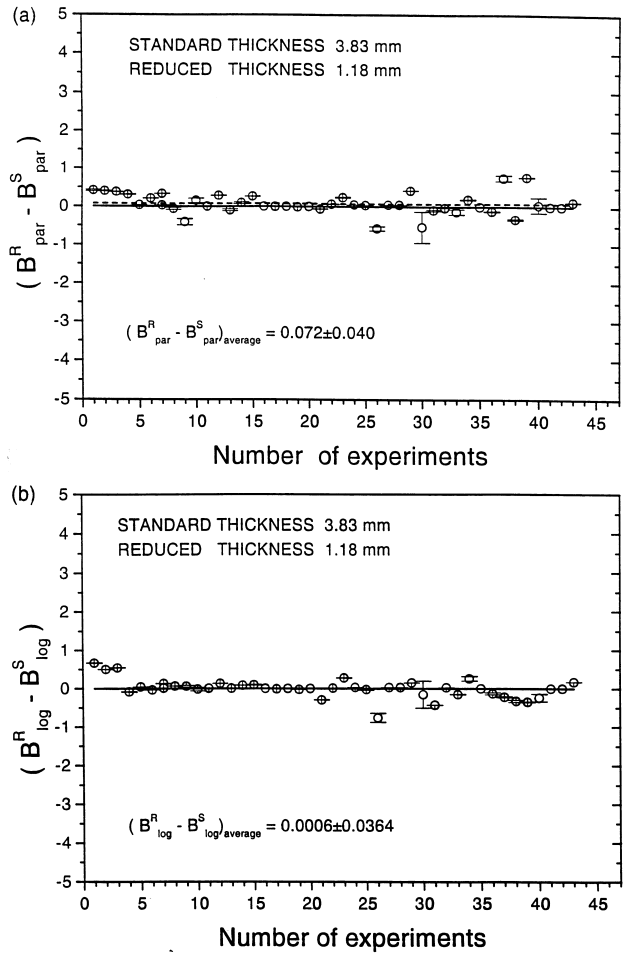

Fig. 11. The difference between the rate constant of the parabolic equation, B_{par} (a), and the logarithmic equation, B_{log} (b), for the LSM specimen of two different thicknesses.

indicates that the gas/solid equilibration process is rate controlled by the diffusion through individual grains (and grain boundaries) rather than by the bulk transport. Concordantly, one may assume that there is a very fast transport of oxygen along grain boundaries and a slow transport of defects that results in reduction of oxygen potential gradient with individual grains. This phenomenon is not surprising as it was observed that the grain boundary diffusion in metal oxides is faster than the bulk diffusion by 5 orders of magnitude [24].

5.3. Diffusion data

The Arrhenius plots of the chemical diffusion coefficient for LSM, determined from Eqs. (3) and (5) during oxidation and reduction experiments, are shown in Fig. 12 along with those reported in literature [1,2,5]. The results of activation energy are given in Table 1. The chemical diffusion coefficient determined in reduction runs from the parabolic equation ($0 < \gamma < 0.5$) exhibits the same activation energy as that determined from the logarithmic equation, even though these two sets of data differ by the factor of about 7, whereas the chemical diffusion coefficient determined for oxidation runs exhibits larger activation energy than that determined during reduction runs. As seen in Table 1 the activation energy for reduction (116–118 kJ mol^{-1}) is lower than that for oxidation (155–196 kJ mol^{-1}). This difference indicates that the equilibration process for the LSM material is faster for reduction than that for oxidation. This effect can be considered in terms of either (i) a surface reaction which is rate controlling the oxidation process, or (ii) the effect of non-stoichiometry on transport.

The first scenario assumes that a surface reaction, such as oxygen incorporation into the boundary layer or its transport across this layer, may be rate controlling the oxidation kinetics while the reduction is bulk diffusion controlled. Concordantly, one could expect that the transport during oxidation is retarded by a segregation-induced diffusive resistance formed by a potential barrier in the boundary layer [25].

The dissimilar oxidation and reduction kinetics may also be considered in terms of essentially different defect structure accompanying oxidation and reduction. As seen from Fig. 1 the predominant defects participating in the transport during the reduction experiments, taking place at low $p(O_2)$, are oxygen vacancies, while at higher oxygen partial pressure (oxidation runs) the transport mainly occurs via cation vacancies. This difference in defect chemistry of the LSM materials during reduction and oxidation runs may be responsible for the difference in the observed equilibration kinetics.

Belzner et al. [1,5] measured the chemical diffusion coefficient of oxygen on $La_{0.79}Sr_{0.20}MnO_{3-\delta}$ and $La_{0.5}Sr_{0.5}MnO_{3-\delta}$ using an electrochemical relaxation method. Although their data exhibit a scatter over the 2 orders of ganitude range, only the data for $La_{0.79}Sr_{0.2}MnO_3$ [1] correspond to practically the same composition as that used in this study. As seen in Fig. 12 there is an outstanding agreements between the data of Beltzner et al. [1] and the chemical diffusion coefficient obtained for reduction using Eq. (3). The diffusion coefficient determined for $La_{0.79}Sr_{0.20}MnO_{3-\delta}$ sample was in the range of $\sim 10^{-7}$ cm^2 s^{-1} at 973 K and of $\sim 10^{-6}$ cm^2 s^{-1} at 1133 K. This corresponds an activation energy of 100–130 kJ mol^{-1}. On $La_{0.5}Sr_{0.5}MnO_{3-\delta}$ composition, the chemical diffusion coefficient was in the range of $\sim 10^{-9}$ cm^2 s^{-1} at 968 K and of $\sim 10^{-7}$ cm^2 s^{-1} at 1113 K. Hammouche et al. [2] also estimated the chemical diffusion coefficient of 4×10^{-8} cm^2 s^{-1} at 1233 K for $(La,Sr)MnO_3$ by an electrochemical relaxation method. Considering the difference in the composition and microstructure of the LSM materials and different techniques used to monitor the equilibration kinetics by different groups, the diffusion data measured by electrochemical relaxation method [1,2,5] can be considered

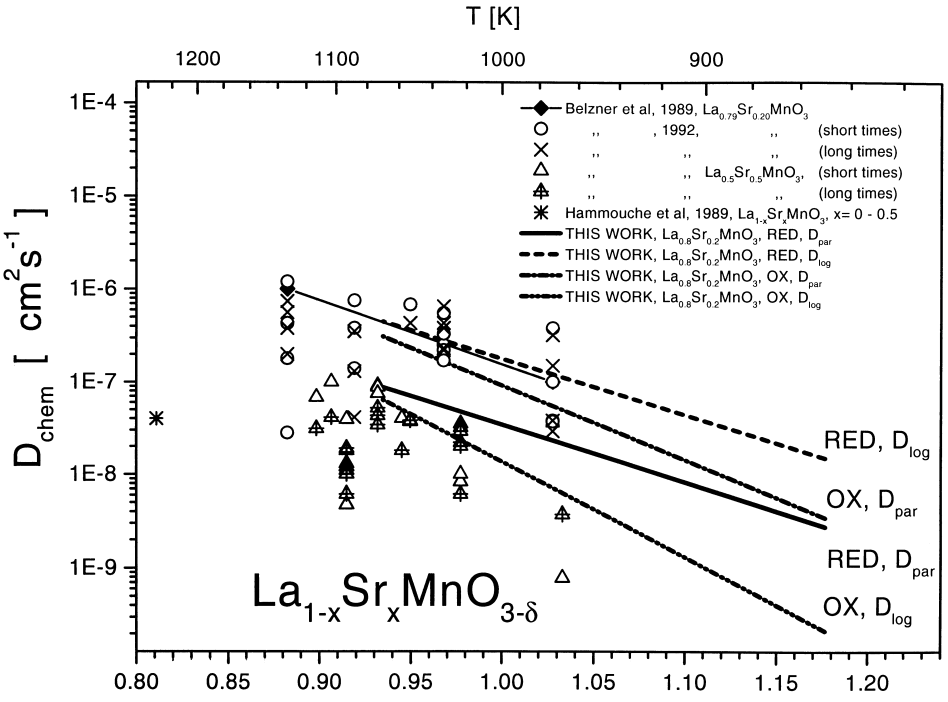

Fig. 12. Arrhenius plot of the chemical diffusion coefficient obtained in this work along with literature data [1,2,5].

Table 1
Activation energy of chemical diffusion

Experiment	Kinetic equation	E_{act} (kJ mol^{-1})
Oxidation	Parabolic	196
	Logarithmic	155
Reduction	Parabolic	119
	Logarithmic	117

to be in the similar range with the one determined by the manometric method in the present study.

6. Conclusions

This paper describes the procedure of the manometric method for the determination of the chemical diffusion coefficient for LSM, which is a certain measure of oxygen transport kinetics. It has been shown that the manometric method applied in this study is a very convenient way of evaluation of the oxygen transport in non-stoichiometric oxide materials such as LSM.

It appears that the chemical diffusion coefficient is strongly dependent on oxygen nonstoichiometry. Accordingly, the chemical diffusion data differ for oxidation and reduction experiments. The diffusion data obtained in this study indicate that the oxygen-ion transport during oxidation exhibits higher activation energy ($E_{par} = 196$ kJ mol^{-1}, $E_{log} = 155$ kJ mol^{-1}) than that during the reduction ($E_{par} = 119$ kJ mol^{-1}, $E_{log} = 117$ kJ mol^{-1}). These data suggest that the oxidation kinetics is either affected by a segregation-induced surface diffusion resistance during oxidation [25] or by different defects concentration accompanying oxidation and reduction.

The activation energy of the chemical diffusion coefficient provide useful information on the possible rate controlling process for the oxygen reduction process in solid oxide fuel cells.

The chemical diffusion data measured by the present manometric method are generally close to that measured by the electrochemical relaxation techniques.

Acknowledgements

The work reported in this paper was supported in part by Ceramic Fuel Cell Limited. This support is gratefully acknowledged. The LSM powder was prepared by Dr. S. Rajendran.

References

[1] A. Belzner, T.M. Gur, R.A. Huggins, in: S.C. Singhal (Ed.), Proceedings of the International Symposium on Solid Oxide Fuel Cells, Vol. 89-11, The Electrochemical Society, Pennington, NJ, 1989, p. 214.

[2] A. Hammouche, E. Siebert, M. Kleitz, A. Hammou, in: S.C. Signhal (Ed.), Proceedings in the International Symposium on Solid Oxide Fuel Cells, Vol. 89-11, The Electrochemical Society, Pennington, NJ, 1989, p. 265.

[3] T. Ishigaki, S. Yamauchi, K. Kishio, J. Mizusaki, K.J. Fueki, Solid State Chem. 73 (1988) 179–187.
[4] B.C.H. Steele, S. Carter, J. Kajda, I. Kontoulis, J.A. Kilner, in: F. Grosz, P. Zeglers, S.C. Singhal, O. Yamamoto (Eds.), Proceedings of the 2nd International Symposium on Solid Oxide Fuel Cells, Commission of the European Communities, Luxembourg, 1991, pp. 517–525.
[5] A. Belzner, T.M. Gur, R.A. Huggins, Solid State Ionics 57 (1992) 327–337.
[6] S. Carter, A. Seluck, R.J. Chater, J. Kajda, J.A. Kilner, B.C.H. Steele, Solid State Ionics 53–56 (1992) 597–605.
[7] I. Yasuda, K. Ogasawara, M. Hishinuma, T. Kawada, M. Dokiya, Solid State Ionics 86–88 (1996) 1197–1201.
[8] M.H.R. Lankhorst, H.J.M. Bouwmeester, J. Electrochem. Soc. 144 (1997) 1261–1267.
[9] J.A.M. Roosmalen, E.H.P. Cordfunke, J. Solid State Chem. 110 (1994) 109–112.
[10] J.A.M. Roosmalen, E.H.P. Cordfunke, J. Solid State Chem. 110 (1994) 113–117.
[11] M.H.R. Lankhorst, H.J.M. Bouwmeester, J. Electrochem. Soc. 144 (1997) 1268–1273.
[12] J.H. Kuo, H.U. Anderson, D.M. Sparlin, J. Solid State Chem. 83 (1989) 52.
[13] J.H. Kuo, H.U. Anderson, D.M. Sparlin, J. Solid State Chem. 87 (1990) 55.
[14] S. Otoshi, H. Sasaki, H. Ohnishi, M. Hase, K. Ishimaru, M. Higuchi, T. Higuchi, M. Miyayama, H. Yanagida, J. Electrochem. Soc. 138 (1991) 1519.
[15] K. Kamata, T. Nakajima, T. Hayashi, T. Nakamura, Mater. Res. Bull. 13 (1978) 49.
[16] H. Kamata, Y. Yonemura, J. Mizusaki, H. Tagawa, K. Naraya, T. Sasamoto, J. Phys. Chem. Solids 56 (1995) 943.
[17] J. Nowotny, M. Rekas, J. Am. Ceram. Soc. 81 (1998) 67.
[18] S.P.S. Badwal, S.P. Jiang, J. Love, J. Nowotny, M. Rekas, J. Austral. Ceram. Soc. 34 (1998) 154.
[19] S.P.S. Badwal, S.P. Jiang, J. Love, J. Nowotny, M. Rekas, J. Austral. Ceram. Soc. 34 (1998) 159.
[20] J.B. Price, J.B. Wagner Jr., Z. Physik. Chem., Neue Folge 49 (1966) 257.
[21] J. Nowotny, M. Rekas, C.C. Sorrell, H.-I. Yoo, J. Austral. Ceram. Soc. 34 (1998) 80.
[22] O.F. Kononchuk, D.P. Sutija, T. Norby, P. Kofstad., in: S.C. Singhal (Ed.), Proceedings of the 1st International Symposium on Solid Oxide Fuel Cells, Vol. 89-11, The Electrochemical Society, Pennington, NJ, 1989, p. 395.
[23] K. Kowalski, E.G. Moya, J. Nowotny, J. Phys. Chem. Solids 57 (1996) 153.
[24] S.P.S. Badwal, K. Foger, Mater. Forum 21 (1997) 183–220.
[25] Z. Adamczyk, J. Nowotny, J. Phys. Chem. Solids 47 (1986) 11–27.